Pergamon

Int. J. Heat Mass Transfer. Vol. 38, No. 15, pp. 2733–2742, 1995

0017-9310/95 $9.50+0.00

0017-9310(95)00040-2

Effect of natural convection on laminar pipe flow solidification

G. J. HWANG and C. W. TSAI

Department of Power Mechanical Engineering, National Tsing Hua University, Hsinchu 30043, Taiwan, Republic of China

(*Received* 15 *August* 1994 *and in final form* 18 *January* 1995)

Abstract—This paper investigates numerically the effect of natural convection on the solidification of laminar fluid flow in the thermal entrance region of a horizontal isothermally cooled tube. The theoretical solution assumes that the Prandtl number is large, and the variation of the liquid–solid interface is gradual in the axial direction. For the liquid phase, a vorticity stream function equation is formulated and solved by a boundary vorticity method. The significance of the natural convection effect is found to depend on the local Rayleigh number. A circular liquid–solid interface is assumed with its center moving up gradually away from the tube axis. The growth of the solid shell is strongly influenced by the superheat ratio λ, the Rayleigh number and the axial position. The theoretical analysis yields the profiles of liquid–solid interface, pressure drop and heat transfer coefficient with varying axial location for the cases of $0 \leqslant Ra \leqslant 10^7$ and $0.1 \leqslant \lambda \leqslant 10$. The numerical predictions agree fairly well with the existing experimental data for the heat transfer rate, the pressure drop and the liquid–solid interface.

1. INTRODUCTION

In the past, a limited amount of research has been done on the subject of liquid solidification inside ducts. Solidification involving the phase-change process is referred to as the moving boundary problem. Usually, those problems encountered in engineering are seldom examined fully analytically. The difficulties arise from the influence of the liquid–solid interface on the flow and heat transfer characteristics of the liquid phase, particularly when the solidification process is accompanied by the effect of natural convection in an internal duct. A literature survey reveals that very little research has been carried out regarding the effect of natural convection on the flow and heat transfer characteristics during the internal solidification.

In 1968, Zerkle and Sunderland [1] presented an experimental and analytical investigation of the effect of solidification on the laminar flow heat transfer and pressure drop in a tube with constant wall temperature. They conducted an experiment using water as a working fluid in a circular tube of 1.5 in diameter and used a parabolic axial velocity profile to obtain the theoretical heat transfer coefficients. Values of the Rayleigh number were of the order of 10^6–10^7. A discrepancy of 100%, based on the theoretical value, was found between the theoretical and experimental heat transfer rates. They suggested that the difference was attributed to the effects of natural convection. Using the empirical formulation developed by Oliver [2], a semi-empirical method taking natural convection into account was presented. Özisik and Mulligan [3] employed a slug flow assumption in an analysis of the transient solidification. Since the slug flow convectively enhances the near-wall heat transfer, the predicted heat transfer coefficients were greater than the ones using a parabolic velocity profile found by Zerkle and Sunderland [1]. Depew and Zenter [4] performed an experiment for the laminar flow heat transfer and the pressure drop with freezing at the wall. A test section of 0.786 in diameter ($L/D = 28.3$) was used with values of the Rayleigh number reaching 10^5–10^6. Similarly, due to the effect of natural convection, the heat transfer rate was 50–80% higher than that using the parabolic velocity assumption. It was also found that the pressure drop was extremely sensitive to the wall temperature and a considerable variation may be found.

Considering a gradual development of the axial uniform velocity to a fully developed one, Hwang and Sheu [5] presented a theoretical and experimental investigation of liquid solidification in the combined hydrodynamic and thermal entrance flow in a circular tube with a uniform wall temperature. An experiment using water as a working medium was carried out to verify the theoretical results. Two double-pipe heat exchangers with small inner-tube diameter of 0.95 cm for suppressing the natural convection effects were employed. The theoretical solution assumed a quasi-steady condition, gradual axial variations in the liquid–solid interface and a significant radial velocity component. A reasonable agreement between their theoretical curves and experimental data was observed. Mulligan and Jones [6] conducted an experiment on the heat transfer and pressure drop in an isothermal horizontal tube of diameter 1.45 cm with internal solidification in the thermal entrance region. The experimental apparatus was designed to make the Graetz number achieve the range of significant natural

NOMENCLATURE

a tube radius [m]
c specific heat of liquid [W kg^{-1}K^{-1}]
D tube diameter $= 2a$ [m]
e dimensionless distance between centre of circular liquid core and tube axis
g gravitational acceleration [m s^{-2}]
Gr Grashof number $= g\beta(T_0 - T_f)a^3/\nu^2$ based on tube radius
Gr_D Grashof number $= g\beta(T_0 - T_f)D^3/\nu^2$ based on tube diameter
k thermal conductivity [W m^{-1}K^{-1}]
Nu Nusselt number $= 2h\,ra(z)/k$
$\bar{p}, p$ pressure in mainstream and cross-stream momentum equations respectively [N m^{-2}]
$\bar{P}, P$ dimensionless pressure in mainstream and cross-stream momentum equations
P^* dimensionless pressure drop $= 2(\bar{p}_0 - \bar{p})/\rho w_0^2$
Pr Prandtl number, ν/α
q, q^* dimensional and dimensionless heat transfer rate $q^* = q/\pi a^2 w_0 \rho c(T_0 - T_f)$
r, ϕ cylindrical coordinates [m], [rad]
R, ϕ dimensionless cylindrical coordinates, $R = r/ra(z)$
$ra(z)$ interface radius [m]
Ra_D, Ra Rayleigh numbers $= PrGr_D$, $PrGr$ respectively
Re Reynolds number $= w_0 D/\nu$
T, T_s, T_w liquid, solid and wall temperatures [K]
w_0 main flow velocity at inlet [m s^{-1}]
u, v, w velocity components [m s^{-1}]
U, V, W dimensionless velocity components
z, Z dimensional and dimensionless axial distances, $Z = (z/a\,Pr\,Re)$.

Greek symbols
α thermal diffusivity [m^2 s^{-1}]
β thermal expansion coefficient, [K^{-1}]
δ dimensionless liquid phase radius, $ra(z)/a$
ζ dimensionless vorticity
η dimensionless radial coordinate in solid phase, r/a
$\eta_i, \eta_o(\phi)$ dimensionless inner and outer boundary of solid respectively
$\eta_i'(\phi)$ present location of solid formation
θ, θ_s dimensionless temperature in liquid and solid respectively
λ super heat ratio $= k_l(T_0 - T_f)/k_s(T_f - T_w)$
ξ dimensionless axial distance $= (4z/DPr\,Re)$
ρ density of fluid [kg m^{-3}]
ψ dimensionless stream function.

Subscripts
D diameter
f freezing point or fully developed condition
l liquid
o inlet
s solid
w wall.

Superscript
′ present location/present state.

Symbols
∇^2 dimensionless Laplace operator $= \{(1/R)(\partial/\partial R)[R(\partial/\partial R)] + (1/R^2)(\partial^2/\partial\phi^2)\}$.

convection effect. It is shown that the Oliver's correlation [2] of combined forced and free convection is applicable when L/D is significantly greater than 50. The article concluded that the correlation is more accurate when the presence of a solid phase thickness is taken into account. In order to correlate properly the solidification data involving the natural convection, the quantity $Gr\,Pr\,L/D$, multiplying the square of the local dimensionless interface radius, was suggested.

Recently, the effect of natural convection on the laminar flow heat transfer and ice formation in an isothermal horizontal tube with freezing have been examined experimentally by Hirata and Hanaoka [7]. They correlated the average Nusselt number with a modified Oliver's empirical formula, implying that the effect of natural convection on Nu is controlled by the dimensionless parameter, $Gr\,Pr$. Experimental data reveal that the mean Nusselt number and the thickness of the ice shell are increased with the increase in the Rayleigh number. Some interesting photographs of ice formation with and without the effect of natural convection were also taken. With a negligible natural convection, the flow passage of the liquid phase is almost circularly formed with its center lying on the axis of the tube. Increasing the Rayleigh number, the cross-sectional shape of the flow passage is also nearly circular with its center moving upwards away from the axis of the tube because of the effect of natural convection.

Although the liquid solidification in a horizontal tube has been studied experimentally for decades, no theoretical solution with the effect of natural convection is available in the literature. The difficulty

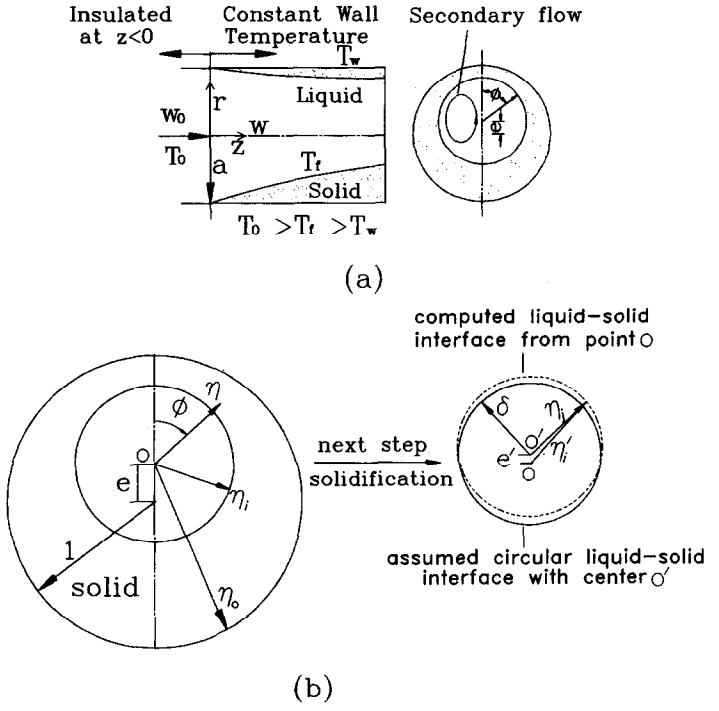

Fig. 1. Physical model and coordinate system.

mainly comes from the complexity of the natural convection flow structure in the liquid phase and the resulting irregularity of the liquid–solid interface. This paper attempts to examine numerically the effect of natural convection on the solidification of laminar pipe flow in the thermal entrance region of a horizontal isothermally cooled tube. The theoretical solution employs the large Prandtl number assumption and considers a small axial variation of the circular liquid–solid interface with its center moving away gradually from the tube axis. With these assumptions, one may expect to obtain a reasonably accurate solution constructed from the available solution in a circular pipe for the liquid phase and the quasi-steady state solution for the solid phase.

2. THEORETICAL ANALYSIS

Consider the laminar mixed convection in the thermal entrance region of a circular tube. Solidification occurs immediately on the tube wall with a uniform temperature below the freezing temperature of the fluid. Due to the secondary flow induced by natural convection, the thickness of the solid is not circumferentially uniform. As depicted in Fig. 1, its cross-sectional shape was found to be nearly circular [7] with its center moving gradually upwards along the flow direction at least in some particular regimes that will be discussed later. The assumption of a circular shape simplifies the problem to one with a fully developed axial flow and 3D parabolic governing equation [8].

A. *Liquid phase*

The following assumptions are made in the theoretical analysis for the liquid flow bounded by the liquid–solid interface.

1. The flow is laminar and incompressible.
2. The fluid physical properties are constant.
3. Axial conduction and viscous dissipation are negligible.
4. Boussinesq approximation is valid.

Without loss of the generality, the pressure distribution in the liquid core of the duct can be expressed as

$$\bar{p}(z)+p(r,\phi,z)$$

where the first term indicates the pressure distribution for the fully developed flow, and the second term is the pressure deviation from the fully developed flow.

For facilitating the analysis in the liquid phase, the solid phase and the interface, one introduces the following dimensionless transformations

$$R=\frac{r}{ra(z)},\quad Z=\frac{z}{a\,Re\,Pr},\quad \delta=\frac{ra(z)}{a}$$

$$w_0'=\frac{w_0}{\delta^2},\quad W=\frac{w}{2w_0'},\quad \theta=\frac{T-T_f}{T_0-T_f}$$

$$U=\frac{uv}{\beta g(T_0-T_f)ra^2}=\frac{u}{2w_0(Gr/Re)\delta^2}$$

$$V=\frac{vv}{\beta g(T_0-T_f)ra^2}=\frac{v}{2w_0(Gr/Re)\delta^2}$$

$$P = \frac{p}{\rho\beta g(T_0 - T_f)ra} = \frac{p}{\rho\, Gr\,\delta(2w_0/Re)^2},$$

$$\bar{P} = \frac{\bar{p}}{\rho Pr(2w_0')^2}$$

where $ra(z)$ is the radius of the assumed circular liquid phase; δ is the dimensionless radius ratio of $ra(z)$ and a; $w_0' = w_0/\delta^2$ signifies the axial varying mean flow; $Re = 2w_0 a/\nu$ is the Reynolds number, $Gr = \beta g(T_0 - T_f)a^3/\nu^2$ is the Grashof number. The r- and ϕ-direction characteristic velocity $\beta g(T_0 - T_f)ra^2/\nu$ and characteristic pressure $\rho\beta g(T_0 - T_f)ra$ can be obtained readily by assuming the same order of magnitudes of the pressure term, viscous term and buoyancy term. It is also noted that the transformation is carried out by considering the gradual movement of the center of the liquid core, i.e. the small eccentricity of the liquid core compared with z.

The governing equations become:

Continuity equation:

$$Gr\,\delta^3\left(\frac{\partial(RU)}{\partial R} + \frac{\partial V}{\partial \phi}\right) + \frac{1}{Pr}\left(\frac{\partial(RW)}{\partial Z} - R \times \left(2W + R\frac{\partial W}{\partial R}\right)\frac{1}{\delta}\frac{d\delta}{dZ}\right) = 0 \quad (1)$$

Z-momentum equation:

$$Gr\,\delta^3\left(U\frac{\partial W}{\partial R} + \frac{V}{R}\frac{\partial W}{\partial \phi}\right) + \frac{1}{Pr}W\left[\frac{dW}{dZ} - \left(2W + R\frac{\partial W}{\partial R}\right)\frac{1}{\delta}\frac{d\delta}{dZ}\right] = -\frac{d\bar{P}}{dZ} + 4\bar{P}\frac{1}{\delta}\frac{d\delta}{dZ} + \frac{Gr\,\delta^5}{Pr\,Re^2}\left[\frac{\partial P}{\partial Z} + \frac{1}{\delta}\frac{d\delta}{dZ}\left(P - R\frac{\partial P}{\partial R}\right)\right] + \nabla^2 W \quad (2)$$

R-momentum equation:

$$Gr\,\delta^3\left(U\frac{\partial U}{\partial R} + \frac{V}{R}\frac{\partial U}{\partial \phi} - \frac{V^2}{R}\right) + \frac{1}{Pr}W\left[\frac{\partial U}{\partial Z} + \left(2U - R\frac{\partial U}{\partial R}\right)\frac{1}{\delta}\frac{d\delta}{dZ}\right] = -\frac{\partial P}{\partial R} + \nabla^2 U - \frac{U}{R^2} - \frac{2}{R^2}\frac{\partial V}{\partial \phi} + \theta\cos\phi \quad (3)$$

ϕ-momentum equation:

$$Gr\,\delta^3\left(U\frac{\partial V}{\partial R} + \frac{V}{R}\frac{\partial V}{\partial \phi} + \frac{UV}{R}\right) + \frac{1}{Pr}W\left[\frac{\partial V}{\partial Z} + \left(2V - R\frac{\partial V}{\partial R}\right)\frac{1}{\delta}\frac{d\delta}{dZ}\right] = -\frac{\partial P}{R\,\partial \phi} + \nabla^2 V - \frac{V}{R^2} + \frac{2}{R^2}\frac{\partial U}{\partial \phi} - \theta\sin\phi \quad (4)$$

energy equation:

$$Ra\,\delta^3\left(U\frac{\partial \theta}{\partial R} + \frac{V}{R}\frac{\partial \theta}{\partial \phi}\right) + W\left(\frac{\partial \theta}{\partial Z} - R\frac{\partial \theta}{\partial R}\frac{1}{\delta}\frac{d\delta}{dZ}\right) = \frac{1}{R}\frac{\partial}{\partial R}\left(R\frac{\partial \theta}{\partial R}\right) + \frac{1}{R^2}\frac{\partial^2 \theta}{\partial \phi^2}. \quad (5)$$

With the small Grashof number and large Prandtl number assumptions [8], the inertia terms caused by the effect of natural convection in momentum equations (2)–(4) and the pressure term with coefficient $(Gr/Pr)(\delta^5/Re^2)$ will vanish. The coefficient $(1/\delta)(d\delta/dZ)$ means the percentage change of liquid-phase radius per unit dimensionless axial length. Since this coefficient is frequently small during the solidification, the terms with the coefficient can be dropped from equations (1)–(5). Therefore, the components U and V do not affect the main flow component W which is fully developed before entering the cooled section. Consequently, the axial variations of axial velocity i.e. $\partial(RW)/\partial Z$ can be neglected from continuity equation (1). This reduces equations (1)–(5) to the following form.

Continuity equation:

$$\frac{\partial(RU)}{\partial R} + \frac{\partial V}{\partial \phi} = 0 \quad (6)$$

Z-momentum equation:

$$0 = -\frac{d\bar{P}_f}{dZ} + \nabla^2 W_f$$

$$W_f = 1 - R^2 \quad (7)$$

R-momentum equation:

$$0 = -\frac{\partial P}{\partial R} + \nabla^2 U - \frac{U}{R^2} - \frac{\partial V}{\partial \phi} + \theta\cos\phi \quad (8)$$

ϕ-momentum equation:

$$0 = -\frac{1}{R}\frac{\partial P}{\partial \phi} + \nabla^2 V - \frac{V}{R^2} + \frac{2}{R^2}\frac{\partial U}{\partial \phi} - \theta\sin\phi \quad (9)$$

energy equation:

$$W_f\frac{\partial \theta}{\partial Z} = \frac{1}{R}\frac{\partial}{\partial R}\left(R\frac{\partial \theta}{\partial R}\right) + \frac{1}{R^2}\frac{\partial^2 \theta}{\partial \phi^2} - Ra\,\delta^3\left(U\frac{\partial \theta}{\partial R} + \frac{V}{R}\frac{\partial \theta}{\partial \phi}\right). \quad (10)$$

Combining equations (8) and (9) by a cross differentiation of the pressure terms, and introducing the dimensionless stream function ψ and vorticity ζ, the final govering equations in dimensionless form for the computation are:

$$\nabla^2\zeta = -\left(\frac{\partial \theta}{\partial R}\sin\phi + \frac{1}{R}\frac{\partial \theta}{\partial \phi}\cos\phi\right) \quad (11)$$

$$\nabla^2\psi = \zeta \quad (12)$$

$$W_f\frac{\partial\theta}{\partial Z}=\left[\frac{1}{R}\frac{\partial}{\partial R}\left(R\frac{\partial\theta}{\partial R}\right)+\frac{1}{R^2}\frac{\partial^2\theta}{\partial\phi^2}\right]-Ra\,\delta^3\left[U\frac{\partial\theta}{\partial R}+\frac{V}{R}\frac{\partial\theta}{\partial\phi}\right] \quad (13)$$

where

$$U=\frac{1}{R}\frac{\partial\psi}{\partial\phi},\quad V=-\frac{\partial\psi}{\partial R}.$$

Both the vorticity equation (11) and the stream function equation (12) are of the elliptic type and energy equation (13) is of the parabolic type. A numerical step by step marching technique [8] will be employed for the liquid-phase solution. It is found that the effect of natural convection depends on the local Rayleigh number $Ra\,\delta^3=\beta g(T_0-T_f)ra^3/\nu\alpha$ defined based on the radius of the assumed circular liquid phase. These equations are subjected to the following boundary conditions:

$$\psi(1,\phi,Z)=\frac{\partial\psi(1,\phi,Z)}{\partial R}=0,\quad 0\leqslant\phi\leqslant\pi,\quad Z\geqslant 0$$

$$\psi(R,\phi,Z)=\zeta(R,\phi,Z)=0,\quad 0\leqslant R\leqslant 1,$$

$$\phi=0\text{ and }\pi,\quad Z\geqslant 0$$

$$\psi(0,\phi,Z)=\zeta(0,\phi,Z)=0\qquad 0\leqslant\phi\leqslant\pi,\quad Z\geqslant 0$$

$$\theta(R,\phi,0)=1\qquad 0\leqslant R<1,\quad 0\leqslant\phi\leqslant\pi$$

$$\theta(1,\phi,Z)=0\qquad 0\leqslant\phi\leqslant\pi,\quad Z\geqslant 0$$

$$\frac{\partial\theta(R,\phi,Z)}{\partial\phi}=0\quad 0\leqslant R\leqslant 1,\quad \phi=0\text{ and }\pi,\quad Z\geqslant 0. \quad (14)$$

B. *Solid phase*

In the present study, the cross-sectional shape of the flow passage is assumed nearly circular with its center moving upwards away from the tube axis. The heat conduction in the solid phase between the tube wall and the liquid–solid interface is examined here. The equation in the solid phase is

$$\frac{1}{r}\frac{\partial}{\partial r}\left(r\frac{\partial T_s}{\partial r}\right)+\frac{1}{r^2}\frac{\partial^2 T_s}{\partial\phi^2}+\frac{\partial^2 T_s}{\partial z^2}=0. \quad (15)$$

Using the additional dimensionless variables

$$\theta_s=\frac{T_s-T_w}{T_f-T_w}\quad\text{and}\quad\eta=\frac{r}{a}$$

and the dimensionless variables used for equations (1) to (5), equation (15) becomes

$$\frac{1}{\eta}\frac{\partial}{\partial\eta}\left(\eta\frac{\partial\theta_s}{\partial\eta}\right)+\frac{1}{\eta^2}\frac{\partial^2\theta_s}{\partial\phi^2}+\frac{1}{(Pr\,Re)^2}\frac{\partial^2\theta_s}{\partial z^2}=0. \quad (16)$$

From the order of magnitude analysis, the conduction terms in the radial, circumferential and axial direction could be roughly estimated by the orders of $1/(1-\delta)^2$, $1/(1-\delta)^2\pi^2$, and $1/(Pr\,Re)^2$ respectively. In addition, the radial temperature gradient is much larger than that in the circumferential direction. Therefore, one could reasonably assume that the heat transfer in the radial direction is dominant. Therefore equation (16) can be reduced to

$$\frac{\mathrm{d}}{\mathrm{d}\eta}\left(\eta\frac{\mathrm{d}\theta_s}{\mathrm{d}\eta}\right)=0$$

$$\text{at}\quad\eta=\eta_i,\quad\theta_s=1;\quad\eta=\eta_o,\quad\theta_s=0. \quad (17)$$

Thus, the temperature distribution in the solid phase is

$$\theta_s=\frac{\ln\eta-\ln\eta_o}{\ln\eta_i-\ln\eta_o} \quad (18)$$

where

$$\eta_o=\eta_o(\phi)=-e\cos\phi+\sqrt{1-e^2\sin^2\phi}. \quad (19)$$

The eccentricity $e=e(Z)$ is the distance of the center of circular flow passage to the tube axis.

C. *Liquid–solid interface*

In the present analysis, a smooth interface is assumed and the steady-state condition prevails, then the energy balance at the interface is:

$$\left.\frac{\partial\theta_s}{\partial\eta}\right|_{\eta=\eta_i}=\frac{\lambda}{\eta_i}\left.\frac{\partial\theta}{\partial R}\right|_{R=1} \quad (20)$$

where

$$\lambda=\frac{k_l(T_0-T_f)}{k_s(T_f-T_w)}$$

is the superheat ratio.

Let $\eta_i'(\phi)$ denote the location at which solid is formed at the present step. With the effect of natural convection, η_i' is no longer circumferentially uniform as depicted in Fig. 1. If the axial step size is small enough, η_i' is pretty much the same as η_i, and we can obtain $\eta_i'(\phi)$ from equation (20)

$$\eta_i'=\eta_i'(\phi)=\eta_o\exp\left(\frac{1}{\lambda(\partial\theta/\partial R)|_{R=1}}\right). \quad (21)$$

Since we assume a circular solid–liquid interface, the new radius of core flow should be figured out at this stage. With η_i' we could calculate the radius of liquid flow passage δ at the present step by

$$\pi\delta^2=\int_0^{2\pi}\frac{\eta_i'^2}{2}\mathrm{d}\phi \quad (22)$$

and the variation of the location of the center of liquid flow passage e' at the present step can be calculated by the method of least square error of the difference of δ and η_j by minimizing $f(e')$ where

$$f(e')=\sum(\eta_j-\delta)^2\quad\text{and}\quad\eta_j=\sqrt{\eta_i'^2-2\eta_i'e'\cos\phi+e'^2} \quad (23)$$

where η_j is the distance of the new center to the location at which solid is formed at the present step. The summation of the square error of the difference

of δ and η_j means the total error originated from choosing a new center of the circular shape.

If we set $(\partial f(e')/\partial e') = 0$, we obtain the value of e' that makes the function f a minimum. The eccentricity e of the center of the liquid core to the tube axis is the accumulation of e' at every ξ.

The local Nusselt number Nu is calculated as

$$Nu = \frac{2hra(z)}{k} = \frac{2}{\pi\theta_b}\int_0^{\pi} -\left.\frac{\partial\theta}{\partial R}\right|_{R=1} d\phi. \quad (24)$$

The dimensionless heat transfer rate q^* from the liquid core to the solid phase at a dimensionless axial position ξ is

$$q^* = \frac{q}{\pi a^2 w_0 \rho c(T_0 - T_f)} = \frac{4}{\pi}\int_0^{\xi}\int_0^{\pi} -\left.\frac{\partial\theta}{\partial R}\right|_{R=1} d\phi\, d\xi \quad (25)$$

and the dimensionless pressure drop within the tube of dimensionless length ξ is

$$P^* = \frac{2(\bar{p}_0 - \bar{p})}{\rho w_0^2} = 16^* Pr^* \int_0^{\xi} \frac{1}{\delta^4} d\xi. \quad (26)$$

3. THEORETICAL SOLUTION

The solution of the present problem can be divided into three main parts i.e. the velocity and temperature distributions in the liquid phase, the temperature profile in the solid phase and the shape of liquid–solid interface. Equations (11) to (14) are the governing equations and the boundary conditions for the fluid flow in the liquid phase. These equations are identical to the equations presented in [8] except the Rayleigh number Ra that appeared in [8] is replaced by the local Rayleigh number $Ra\delta^3$ here. One can refer to the work [8] for a detailed solution. The solution of the temperature distribution in the solid phase can be directly calculated from equations (18) and (19).

The interface equation (20) needs complete information on the temperature distributions in both the liquid and solid phases. After the distribution of the liquid-phase temperature is obtained, equation (21) gives the interface location $\eta_i'(\phi)$ at the present step. To validate the assumption of circular-flow, the radius of the liquid–solid interface δ at the present step is derived from equation (22). The eccentricity e of the center of liquid-flow is an accumulation of e' at each step derived from equation (23).

4. RESULTS AND DISCUSSIONS

Figure 2 shows the variations of the dimensionless radius of circular interface δ with the dimensionless axial position ξ for $\lambda = 0.1$–10 and $Ra = 0$–10^7. $\lambda = [k_l(T_0 - T_f)]/[k_s(T_f - T_w)]$ is the superheat ratio. The solid shell grows faster for smaller λ. When $\lambda = 0.1$, no appreciable natural convection effect on the interface radius δ is detected for $Ra = 0$–10^6. This

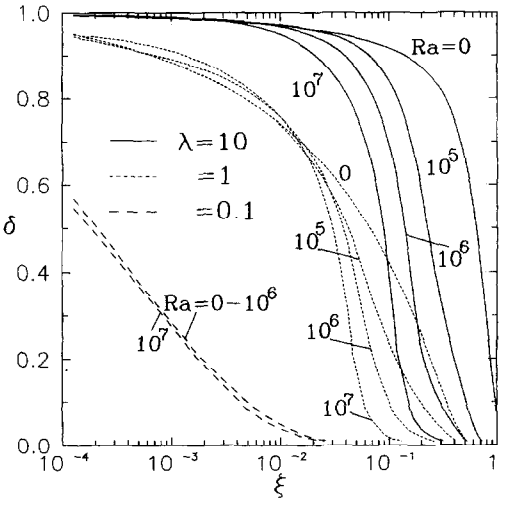

Fig. 2. Dimensionless radius of the liquid–solid interface.

is caused by the rapid decrease of δ and the value of local Rayleigh number $Ra\delta^3$, which reduces the effect of natural convection. As λ increases, the slow growth of the solid phase makes the local Rayleigh number $Ra\ \delta^3$ not decrease too much and thus the effect of natural convection persists. For $\lambda = 1$ and $\xi \leqslant 10^{-2}$, the larger Ra prevents the growth of the solid shell, but, as ξ increases, the fluid temperature drops and δ decreases more rapidly for larger Ra. This phenomenon is in consistent with the statements of [6] and [7]. Reference [6] claims that "natural convection tends to reduce the solid phase thickness and correspondingly, reduces the pressure drop for all but the very small Graetz numbers". Reference [7] states that "for combined forced- and natural-convection flow in a tube with internal freezing, the mean Nusselt number increases and the ice becomes thicker as compared with the results without natural convection". This is because a secondary vortex has been generated by natural convection [8], which makes hotter fluid near the core region move to the cold-wall region. As ξ is small, the mixing effect caused by a secondary vortex results in a higher temperature of the fluid near the wall region than that without natural convection, which tends to decrease the thickness of the solid and gives a larger δ. As fluid flows downstream, on account of the decay of the strength of the secondary vortex, cold fluid will have stagnated near the bottom part of the liquid core and accordingly solidification will occur very quickly there. This phenomenon is more significant with larger Ra.

Figure 3 shows the dimensionless eccentricity e with the dimensionless axial position ξ for $\lambda = 0.1$–10 and $Ra = 0$–10^7. The value of e is the distance of the center of the liquid core to the tube axis. The liquid core moves upwards if $e > 0$ and *vice versa*. Without considering the effect of natural convection, the value of e will be zero. With natural convection, as described before, cold fluid could be trapped in the bottom part of the liquid core and solidify there. So, the liquid core

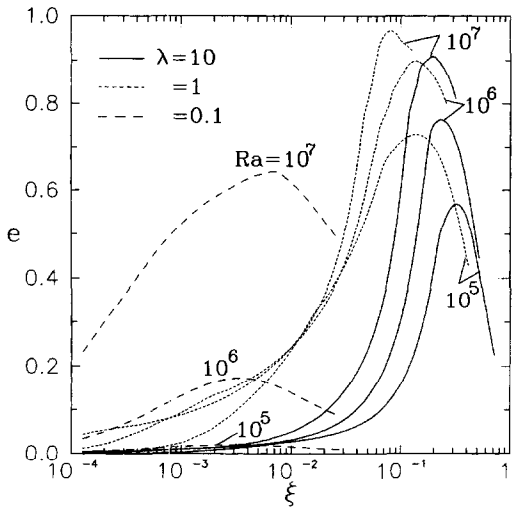

Fig. 3. Dimensionless eccentricity vs axial distance.

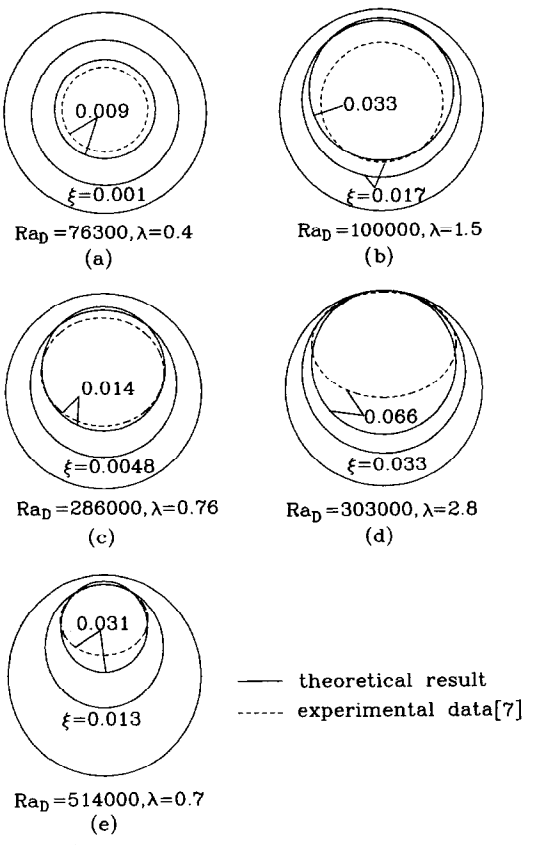

Fig. 4. Comparison of the experimental and theoretical radius of the liquid–solid interface.

always moves upwards. For $\lambda = 0.1$ and $Ra \leqslant 10^5$, the effect of natural convection is negligibly small and the value of e is approximately zero. Generally speaking, this plot shows that the center of the liquid core first moves up to a maximum value then moves down with increasing ξ. This is probably because of the decay of the vortex strength during the last stages of solidification with small δ, and the radial heat conduction of the solid phase dominates the morphology of solidification, which tends to equalize the circumferential thickness of the solid.

Although the present analysis uses the Boussinesq approximation and large Prandtl number assumption and assumes a circular liquid–solid interface, comparisons of liquid–solid interface between the present prediction and the experimental water data [7] are made in Fig. 4(a)–(e). The large Prandtl number assumption can be valid for water ($Pr = 10$) [9]. For most fluids, a linear variation of fluid density with temperature can be acceptably assumed. However, for the case of water near its freezing point a linear relationship is not justified. The anomalous behavior of water results in a rather peculiar convective motion when the temperature domain encompasses the maximum density point near 4°C [10]. This produces an additional complexity in the behavior of the natural convection particular in the internal solidification. For example, instead of the familiar unicellular pattern, the flow may become bicellular with counter direction [11, 12]. To avoid rigorous treatment of the variations of the thermal expansion coefficients β, an estimate of the effective β of the flow encompassing the whole domain between the inlet and outlet should be made. If the outlet bulk fluid temperature is over 4°C, a mean thermal expansion coefficient based on the mean temperature of the inlet and outlet bulk fluid temperature is suggested and substituted for the inlet Rayleigh number to account for the decrease of β in the water flow system. A good reason for this suggestion is that a fluid with a large Prandtl number exhibits inherent characteristics such as a thinner thermal boundary layer of the flow. So the temperature distribution of the flow is flatter and most of the region is very close to the bulk fluid temperature. Accordingly, a representative of β estimated from the bulk fluid temperature is believed to be accurate. Thus the mean β is chosen to represent the effective β covering the whole domain from the inlet to the outlet. If the outlet bulk fluid temperature is over 4°C, a rough calculation for the relative error of the mean β from the effective β is

$$\frac{\beta_m - (\int_1^2 \beta \, dT)/T}{\beta_m}$$

where m, 1, and 2 represent mean, inlet and outlet respectively. Note that a small error of no more than 5% is observed for an inlet water temperature above 10°C.

To take account of the effect of density inversion of water on natural convection, it is better to use the mean Rayleigh number [1, 4–7] to exploit the effect of natural convection

$$Ra_D = \frac{g\beta_m(T_m - T_f)D^3}{\nu^2}$$

where T_m and β_m is measured from the mean value of

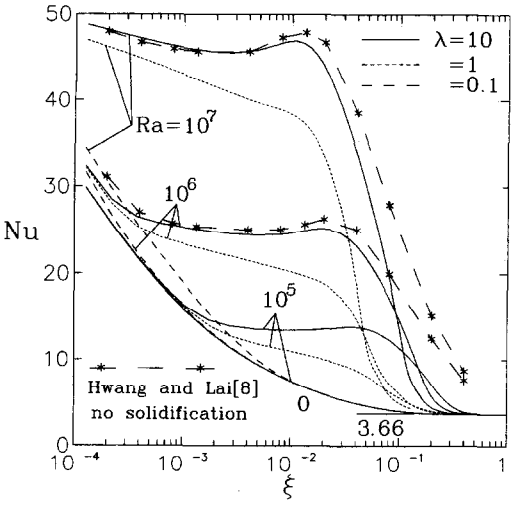

Fig. 5. Theoretical Nusselt number.

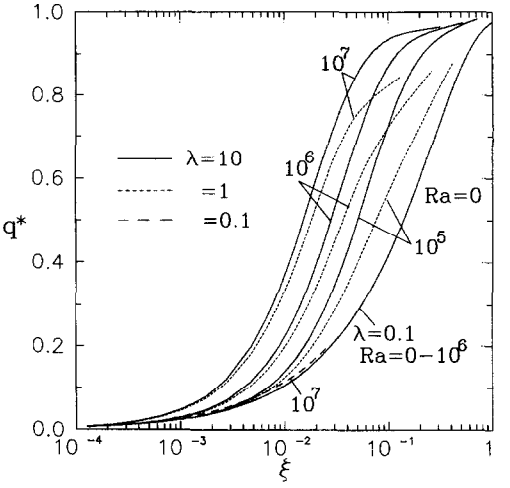

Fig. 6. Dimensionless heat transfer rate.

the inlet and outlet bulk fluid temperature. The mean Rayleigh number is substituted for the inlet Rayleigh number used in the present study for calculation. It is shown that the predicted shapes of the interface plotted in Fig. 4 are qualitatively coincident with the experimental data. For weak natural convection secondary flow, i.e. small Rayleigh number, as shown in (a), (b) and (c), the cross-section of the liquid–solid interface maintains a circular form. It deforms gradually into an elliptic shape as the Rayleigh number increases as shown in (d) and (e), and the center of liquid core moves up much further away from the tube axis. It is seen that the confirmation is satisfactory for cases (a) and (c) with small Ra and λ.

Figure 5 shows the variation of the local Nusselt number Nu with the dimensionless axial position ξ for $\lambda = 0.1$–10 and $Ra = 0$–10^7. The results of Nu presented in [8] for the case without solidification are also plotted. It can also be seen that the Nusselt number increases with the increase in Ra for a fixed λ or with the increase in λ for a fixed Ra. The strong influence of natural convection on Nu is found for $\lambda = 1$ and 10 when $Ra \geqslant 10^6$. For $\lambda = 0.1$, only a small increase of Nu has been found for $Ra = 10^7$. The value of λ shows no effect on Nu for $Ra = 0$. For the case of $\lambda = 10$, the present predictions of Nu are very similar to those of Hwang and Lai [8] for $Ra = 10^7$ and 10^6 in the region of $\xi \leqslant 10^{-2}$. This is because of the thin solid shell, which behaves much the same as in the case without solidification. When $\xi \geqslant 10^{-2}$ the predicted Nu is less than that of Hwang and Lai [8] because of the thick solid shell.

The variation of dimensionless heat transfer rate q^* with the dimensionless axial position ξ for $\lambda = 0.1$–10 and $Ra = 0$–10^7 is shown in Fig. 6. It reveals that there are significant effects of superheat ratio λ and Rayleigh number Ra on the dimensionless heat transfer rate q^*. The value of λ also shows no effect on q^* for the case of $Ra = 0$. For $\lambda = 1$ and 10, q^* increases with increase in Ra. The enhancement of q^* is more pronounced for large λ, which is similar to the case shown in Fig. 5.

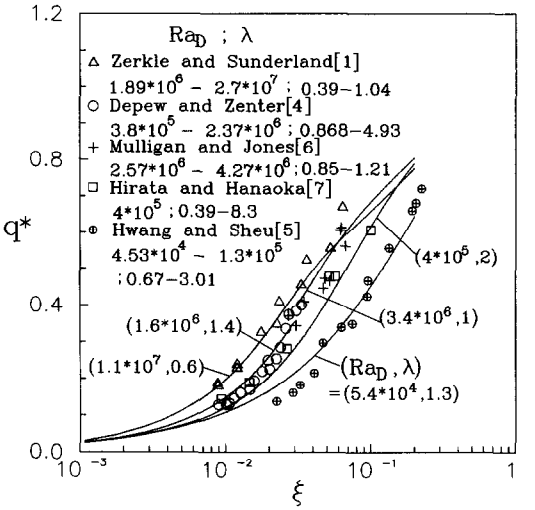

Fig. 7. Comparison of experimental and theoretical heat transfer rates.

Comparisons of the predicted q^* and the experimental water data are made in Fig. 7. The ranges of operating conditions for Ra_D and λ in the experiments [1, 4–7] are also listed in this figure. Since the operating range is wide, the mean values of Ra_D and λ are used in the calculations. From this figure, one sees that the agreement between the present prediction of q^* and the experimental data are quite satisfactory. It is worth mentioning that the value of Ra_D claimed in [6] was overestimated since both the mean fluid temperature (T_m) and inner tube diameter (D) are smaller than those given in ref. [4].

The variations of the dimensionless pressure drops P^* with the dimensionless axial position ξ for $\lambda = 0.1$–

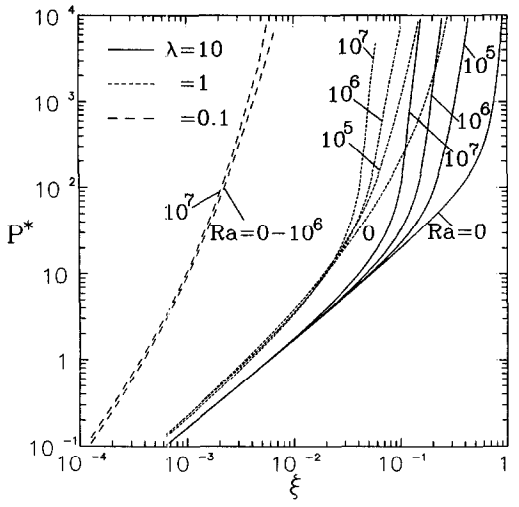

Fig. 8. Theoretical pressure drop.

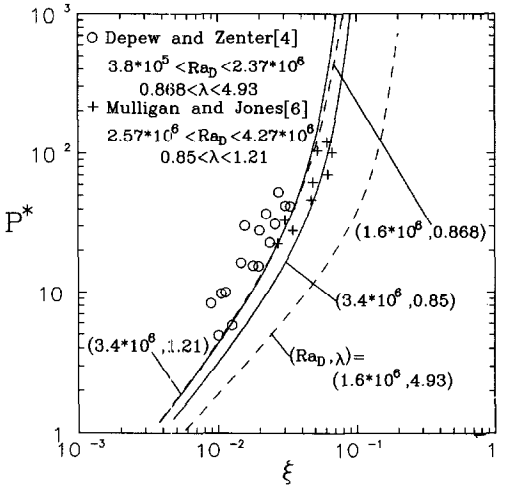

Fig. 9. Comparison of experimental and theoretical pressure drop.

10 and $Ra = 0$–10^7 are depicted in Fig. 8. For calculating the dimensionless pressure drop the value of Pr should be assigned. In order to compare the predicted results of P^* with the experimental data presented in [4, 6] $Pr = 10$ is selected for calculation of equation (26) in Figs. 8 and 9. When Pr is fixed, the pressure drop increases with the decrease in δ. From this figure, one sees that for a fixed Ra, P^* increases with the decrease in λ.

Comparisons of the predicted P^* with the experimental water data [4, 6] are plotted in Fig. 9. The operating ranges of these experiments are also listed in this figure. Prediction has been plotted by four curves. Since P^* is very sensitive to λ, lower and upper limits of λ are used to calculate P^* while the Rayleigh numbers Ra_D are kept fixed to a mean value. Solid lines represent the prediction for the case of [6] and dashed lines for the case of [4]. Figure 9 reveals that the predicted P^* is very close to the data of [6] while a somewhat large deviation from the results of [4] is observed.

5. CONCLUSIONS

1. The present investigation successfully solves the solidification of laminar pipe flow in the thermal entrance region of a horizontal isothermally cooled tube under the effect of natural convection. The theoretical solution employes the large Prandtl number assumption and considers a gradual axial variation of the circular liquid–solid interface with its center moving away from the tube axis. With these assumptions, one is able to obtain a reasonably accurate solution constructed from the available solution in a circular pipe for the liquid phase and from the quasi-steady-state solution for the solid phase.

2. For smaller superheat ratio $\lambda(= 0.1)$, the value of local Rayleigh number $Ra\ \delta^3$ decreases faster because of the rapid growth of the solid shell, which suppresses the effect of natural convection on the dimensionless radius of circular interface δ, while pronounced difference in δ for various Ra can be noticed for cases of larger λ ($= 1$ and 10) for which the effect of natural convection persists. The center of the liquid core moves upwards with the effect of natural convection. This is confirmed by experimental observation.

3. There are significant effects of λ and Ra on the Nusselt number Nu and dimensionless heat transfer rate q^*. The values of Nu and q^* increase with the increase in Ra for the cases of larger λ ($= 1$, 10), but no obvious difference is shown for $\lambda = 0.1$. The value of λ shows no effect on Nu and q^* for $Ra = 0$. The dimensionless pressure drop P^* increases with decrease in λ for a fixed Ra and increases with increasing Ra for a fixed λ.

REFERENCES

1. R. D. Zerkle and J. E. Sunderland, The effect of liquid solidification in a tube upon laminar flow heat transfer and pressure drop, *J. Heat Transfer* **90,** 183–190 (1968).
2. D. R. Oliver, The effects of natural convection on viscous-flow heat transfer in horizontal tubes, *Chem. Engng. Sci.* **17,** 335–360 (1962).
3. M. N. Özisik and J. C. Mulligan, Transient freezing of liquids in forced flow inside circular tube, *J. Heat Transfer* **91,** 385–390 (1969).
4. C. A. Depew and R. C. Zenter, Laminar flow heat transfer and pressure drop with freezing at the wall, *Int. J. Heat Mass Transfer* **12,** 1710–1714 (1969).
5. G. J. Hwang and J. P. Sheu, Liquid solidification in combined hydrodynamic and thermal entrance region of a circular tube, *Can. J. Chem. Enging.* **54,** 66–71 (1976).
6. J. C. Mulligan and D. D. Jones, Experiments on heat transfer and pressure drop in a horizontal tube with internal solidification, *Int. J. Heat Mass Transfer* **19,** 213–219 (1976).
7. Tetsuo Hirata and Chihiro Hanaoka, Laminar-flow heat transfer in a horizontal tube with internal freezing

(effects of flow acceleration and natural convection), *Heat Transfer—Jap. Res.* **19,** 376–390 (1990).
8. G. J. Hwang and H. C. Lai, Laminar convective heat transfer in a horizontal isothermal tube for high Rayleigh number, *Int. J. Heat Mass Transfer* **37,** 1631–1640 (1994).
9. K. C. Cheng and J. W. Ou, Free convection effects on Graetz problem for large Prandtl number fluids in horizontal tubes with uniform wall heat flux, *Proc. 5th International Heat Transfer Conference*, Vol. 3, 159–163 (1974).
10. B. Gebhart and J. C. Mollendorf, Buoyancy-induced flows in water under conditions in which density extrema may arise, *J. Fluid Mech.* **89,** part 4, 673–707 (1978).
11. R. R. Gilpin, Cooling of a horizontal cylinder of water through its maximum density point at 4°C, *Int. J. Heat Mass Transfer* **18,** 1307–1315 (1975).
12. K. C. Cheng and M. Takeuchi, Transient natural convection of water in a horizontal pipe with constant cooling rate through 4°C, *J. Heat Transfer* **98,** 581–587 (1976).